

Supporting Information for

Ga-doped Pt-Ni Octahedral Nanoparticles as a Highly Active and Durable Electrocatalyst for Oxygen Reduction Reaction

*JeongHoon Lim¹, Hyeyoung Shin², MinJoong Kim¹, Hoin Lee¹, Kug-Seung Lee³, YongKeun Kwon¹, DongHoon Song¹, SeKwon Oh¹, and Hyungjun Kim^{4,5}, EunAe Cho^{*1}*

¹Department of Materials Science and Engineering, Korea Advanced Institute of Science and Technology (KAIST), 291 Daehak-ro, Yuseong-gu, Daejeon, 34141, Republic of Korea

²Materials and Process Simulation Center (MSC), California Institute of Technology, Pasadena, California 91125, United States

³Pohang Accelerator Laboratory (PAL) & National Institute for Nanomaterials Technology (NINT), Pohang University of Science and Technology (POSTECH), Pohang 790-784, Republic of Korea

⁴Graduate School of Energy, Environment, Water and Sustainability (EEWS), Korea Advanced Institute of Science and Technology (KAIST), 291 Daehak-Ro, Yuseong-Gu, Daejeon, 34141, Republic of Korea

⁵Department of Chemistry, Korea Advanced Institute of Science and Technology (KAIST), 291 Daehak-Ro, Yuseong-Gu, Daejeon, 34141, Republic of Korea

Table S1. Chemical compositions of the various metals doped onto PtNi/C (M-PtNi/C) as confirmed by ICP-OES.

Catalyst	At %			Pt / Ni
	Pt	Ni	M	
PtNi/C	63.5	36.8	-	1.7
Ga-PtNi/C	62.8	35.7	1.4	1.8
Ru-PtNi/C	65.3	33.7	1.0	1.9
Zr-PtNi/C	63.7	35.2	1.1	1.8
Gd-PtNi/C	66.4	33.4	0.2	2.0
Bi-PtNi/C	64.0	33.6	2.5	1.9
Zn-PtNi/C	61.7	36.9	1.3	1.7
Pb-PtNi/C	65.2	33.0	1.8	2.0

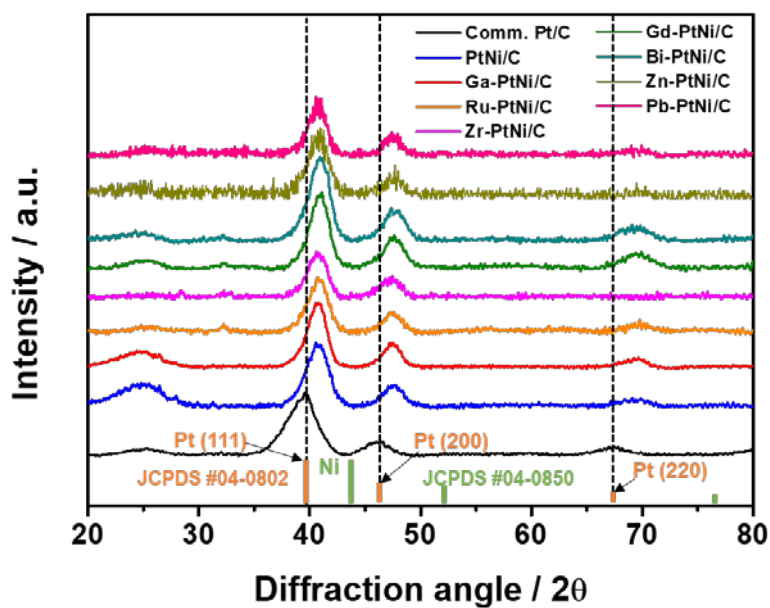


Figure S1. PXRD patterns of commercial Pt/C, PtNi/C and various metals doped onto PtNi/C (M-PtNi/C).

Table S2. Lattice parameters of the commercial Pt/C, PtNi/C, and Ga-PtNi/C from the ideal Vegard's law (unit: Å).

	Commercial Pt/C	PtNi/C	Ga-PtNi/C
hkl	d	d	d
111	2.27	2.22	2.20
200	1.95	1.93	1.91
220	1.38	1.36	1.34

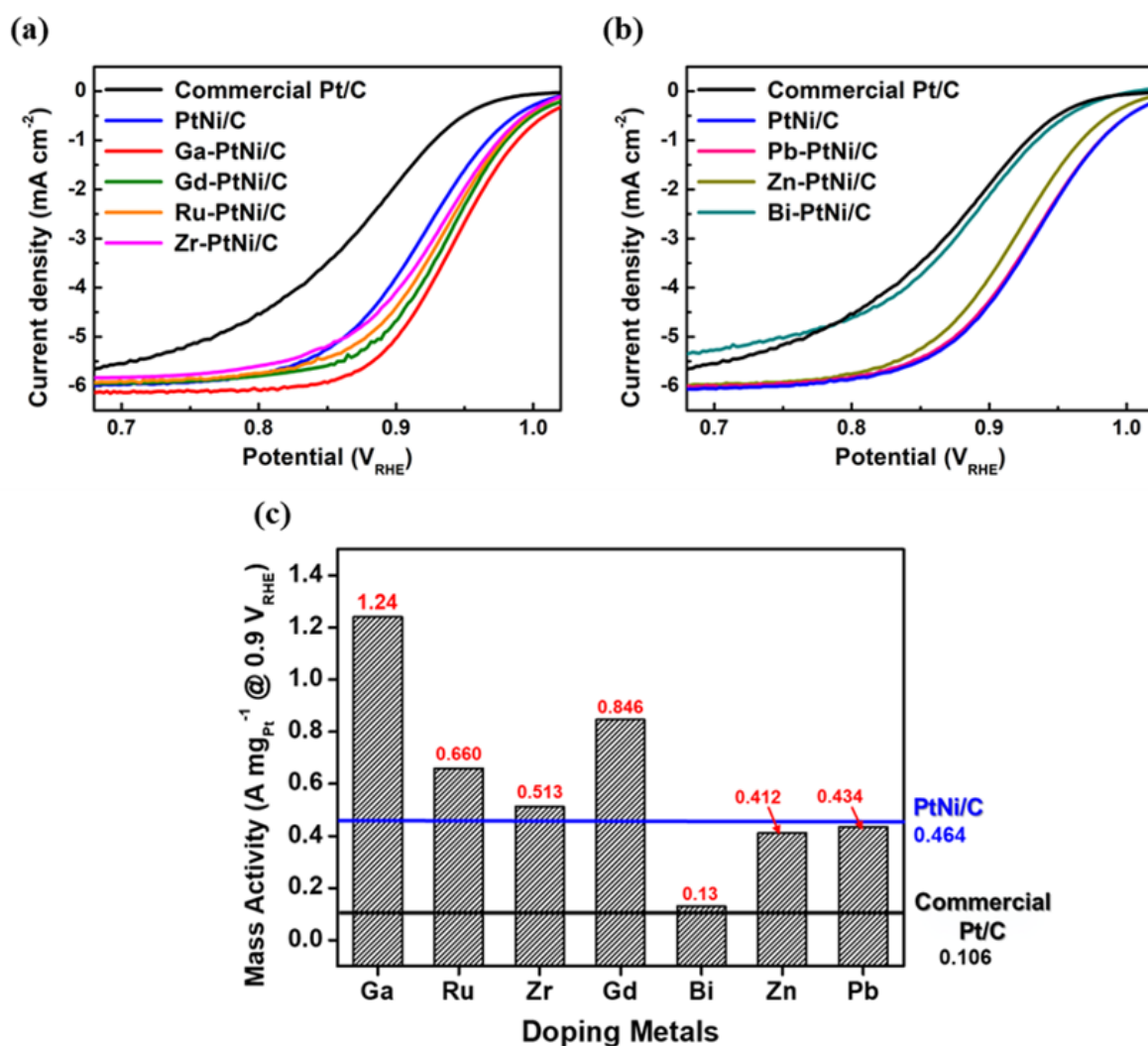


Figure S2. ORR activities of various metals doped onto PtNi/C were measured in O₂-saturated 0.1M HClO₄ with a 10 mV s⁻¹ scan rate at a rotating speed of 1600 rpm: (a) positive effect for ORR activity of the M-PtNi/C (M: Ga, Ru, Zr and Gd); (b) negative effect for ORR activity of the M-PtNi/C (M: Bi, Zn, and Pb); (c) mass activities of the M-PtNi/C, PtNi/C, and commercial Pt/C (Tanaka Co.) are summarized.

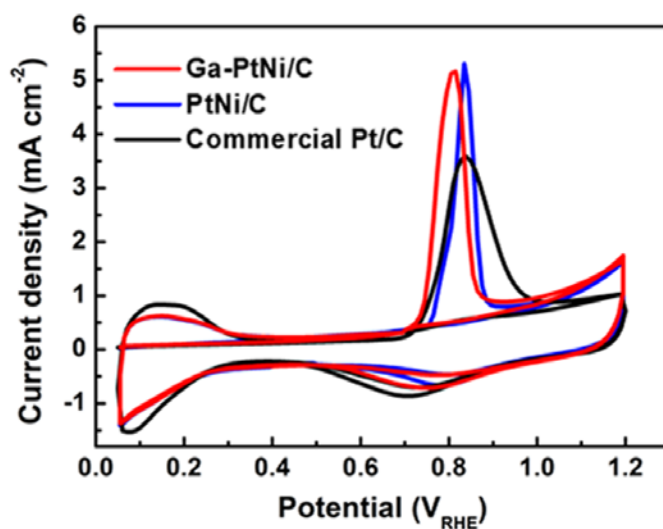


Figure S3. CO-stripping experiment with Ga-PtNi/C, PtNi/C, and commercial Pt/C carried out in CO-saturated 0.1 M HClO₄ electrolyte at room temperature with a scan rate of 50 mV s⁻¹.

Table S3. ECSA values as estimated by the integrated charge from the CO adsorption peak area (CO_{ad}).

	ECSA _{CO} (m ² g _{Pt} ⁻¹)
Ga-PtNi/C	53
PtNi/C	53
Commercial Pt/C	78

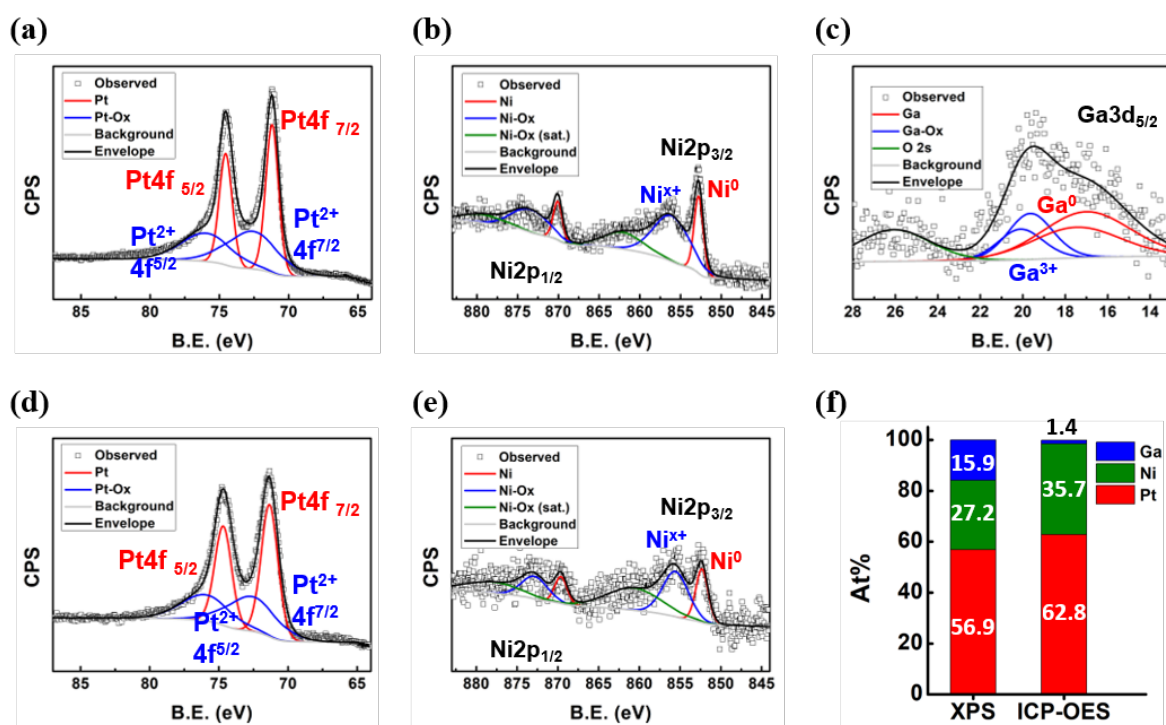


Figure S4. Surface characterization according to an XPS analysis of pristine Ga-PtNi/C and PtNi/C: (a) Pt spectra, (b) Ni spectra, and (c) Ga spectra of Ga-PtNi/C, (d) Pt spectra and (e) Ni spectra of PtNi/C. (f) Composition of Pt, Ni, and Ga in Ga-PtNi measured by XPS and ICP-OES. The Pt 4f, Ni 2p, and Ga 3d peaks of Ga-PtNi/C and PtNi/C reveal that most of Pt was in a metallic state, most of Ni was in an oxidized state and Ga was in a metallic state and a Ga³⁺ state.

Table S4. Literature survey for the accelerated degradation test conditions of doping onto Pt-based catalysts.

Catalysts	Doping metals	Mass activity (A/mg _{Pt} @ 0.9 V _{RHE})	Durability test conditions			
			Number of cycles	Purging gas	Scan rate (mV/s)	Potential range (V _{RHE})
Fe-PtNi NPs ¹	Fe	0.37	16k	Not given	50	0.6~1.1
Mo-PtNi/C ²	V, Cr, Mn, Fe, Co, Re, W, Mo	6.98	8k	O ₂	50	0.6~1.1
Br-PtNi/C ³	Halide (F, Cl, Br, I)	0.37	10k	O ₂	100	0.6~1.1
Au-PtCu/C ⁴	Au	Not given	10k	Not given	1000	0.4~1.2
Rh-PtNi NPs ⁵	Rh	1.14	30k	deaerated electrolyte	100	0.6~1.0
<i>This work</i>	<i>Ga</i>	<i>1.33</i>	<i>30k</i>	<i>O₂</i>	<i>50</i>	<i>0.6~1.1</i>

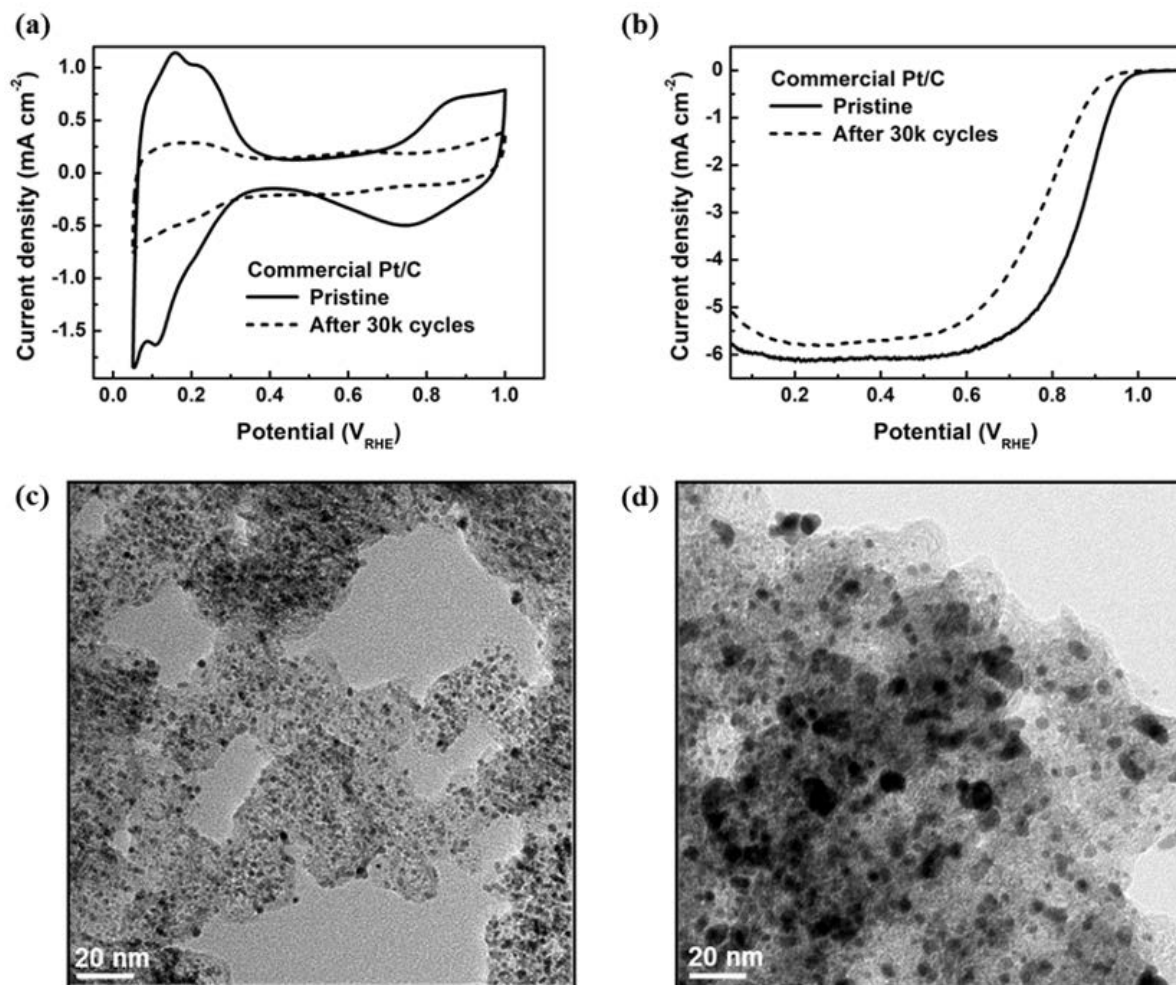


Figure S5. Long-term durability test of the commercial Pt/C (Tanaka Co. 46 wt%): (a) CV curves of Pt/C before and after 30k cycles, (b) ORR polarization curves of Pt/C before and after 30k cycles. TEM images of Pt/C (c) before and (d) after 30k cycles. The durability test was carried out in an O₂-purged condition in a 0.1M HClO₄ electrolyte between 0.6-1.1 V_{RHE} with a scan rate of 50 mV s⁻¹.

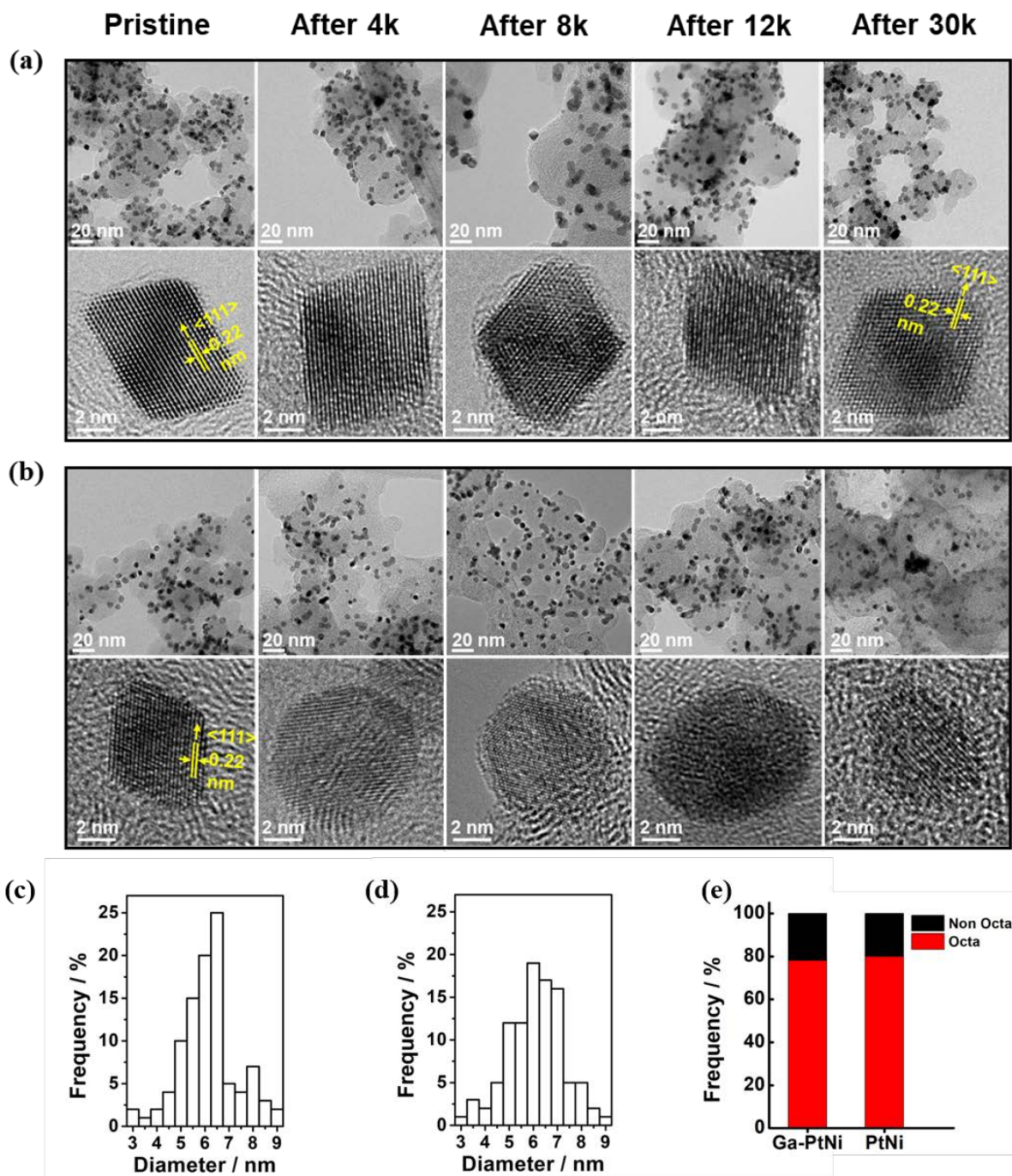


Figure S6. HR-TEM images with regard to the shape stability and nanoparticle distributions of (a) Ga-PtNi/C and (b) PtNi/C in a pristine condition and in durability tests at 4k, 8k, 12k, and 30k cycles. Nanoparticle size distribution of (c) Ga-PtNi/C and (d) PtNi/C. The ratio of Octahedral and not octahedral shape nanoparticles of Ga-PtNi and PtNi was described in (e).

For the durability test of (a) Ga-PtNi/C up to 30k cycles, the majority of octahedral nanoparticles showed high shape stability and were well dispersed on the carbon support with an average size of approximately 6.0 ± 0.4 nm during the durability test. On the other hand, the PtNi octahedral nanoparticles of PtNi/C lost their octahedral shape and became spherically shaped with severe agglomeration after a durability test of only 4k cycles. The average sizes of the nanoparticles size are around 6.2 nm (4k), 6.5 nm (8k), 6.7 nm (12k), and 6.8 nm (30k).

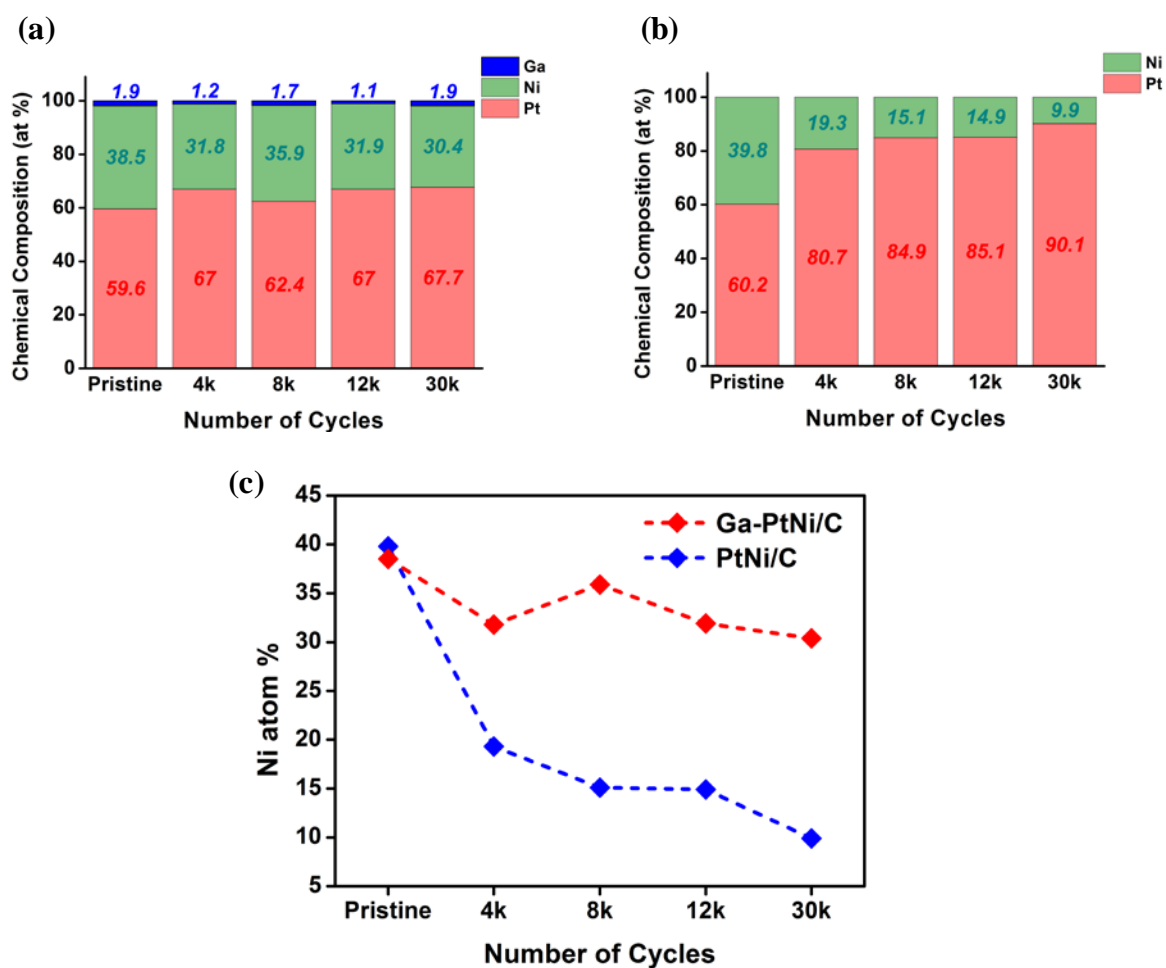


Figure S7. Chemical composition changes as confirmed by EDX to compare the Pt and Ni atomic percentages in individual nanoparticles of (a) Ga-PtNi/C and (b) PtNi/C, and (c) changes of Ni atoms in the nanoparticles during the durability test.

Table S5. Pt, Ni, and Ga concentrations in the electrolytes of Ga-PtNi/C and PtNi/C after a 30k cycle durability test as measured by ICP-MS (unit: ppb ($\mu\text{g} / \text{kg}$)).

	Ga-PtNi/C	PtNi/C
Pt	1.5	2.7
Ni	5.0	34.3
Ga	0.3	-

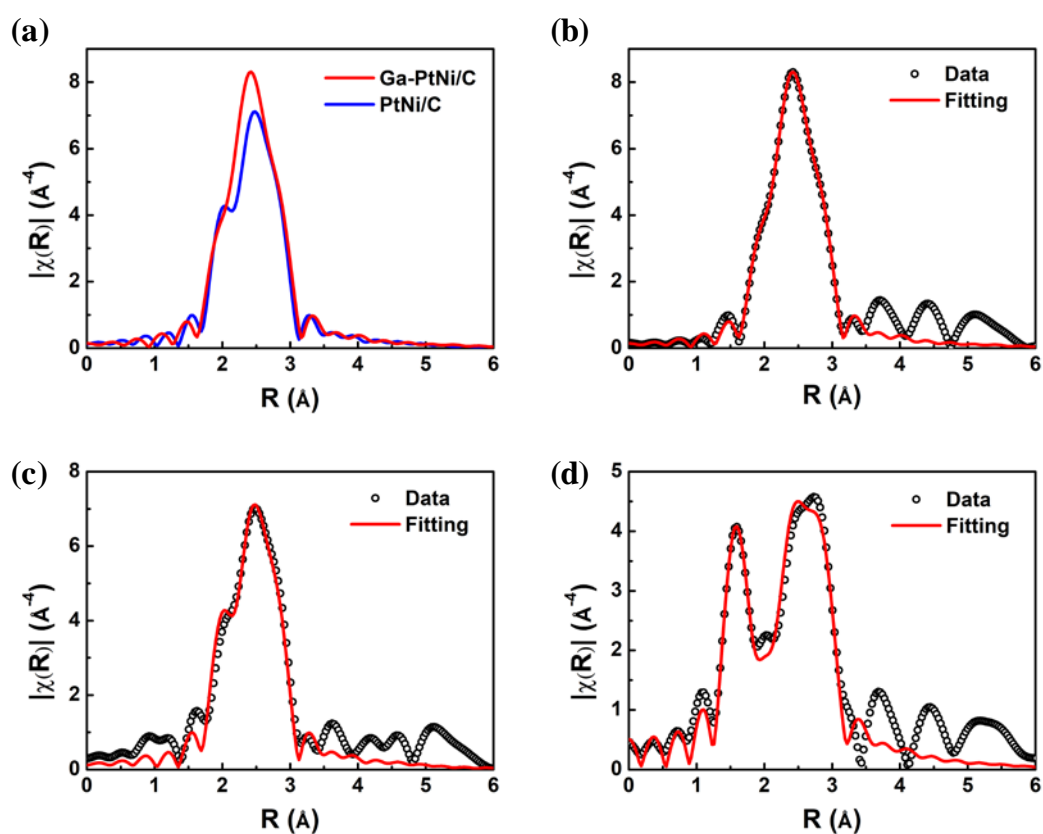


Figure S8. Fourier-transforms of k^3 -weighted EXAFS spectra (circle) and their best fits (red solid line): (a) Pt L3-edge of Ga-PtNi/C and PtNi/C and EXAFS data fitting results of (b) Ga-PtNi/C, (c) PtNi/C, and (d) Pt/C.

Table S6. Summary of the EXAFS fitting results of Ga-PtNi/C, PtNi/C, and commercial Pt/C

Sample	Path	N	R (Å)	σ^2 (Å ²)	R-factor (%)
Ga-PtNi/C	Pt-Ni	2.8 ± 0.5	2.620 ± 0.011	0.010 ± 0.001	0.2
	Pt-Pt	7.5 ± 0.6	2.719 ± 0.003	0.007 ± 0.001	
PtNi/C	Pt-Ni	2.6 ± 1.5	2.619 ± 0.039	0.013 ± 0.005	1.5
	Pt-Pt	7.0 ± 1.7	2.723 ± 0.008	0.007 ± 0.001	
Pt/C	Pt-O	1.8 ± 0.4	2.003 ± 0.018	0.003 ± 0.002	1.4
	Pt-Pt	6.0 ± 1.3	2.747 ± 0.011	0.007 ± 0.001	

(N = coordination number, R = interatomic distance, σ^2 = Debye-Waller factor (bond disorder), R-Factor = a measure of the quality of the EXAFS fit).

Computational Details

In the present work, spin-polarized density functional theory (DFT) calculations were carried out within the plane-wave basis set and projector augmented wave (PAW)⁶ framework, as implemented in Vienna Ab-initio Simulation Package (VASP).⁷ RPBE⁸ functional was used and the plane-wave energy cutoffs were set as 450 eV. For each surface slab model, (4×4) *fcc* (111) periodic slab models of three metal layers with 20 Å vacuum spacing and 48 atoms were employed and only the topmost two layers were allowed to relax whereas one bottom layer was fixed at the lattice point to approximate the bulk. (5×5×1) gamma k-point mesh was utilized. Furthermore, dipole correction was applied along the normal direction toward the surface and an implicit Poisson-Boltzmann solvation method⁹ was used to describe the water solvation energies (the dielectric constant was set as 80).

The atomic ratio of Pt to Ni was set as 2.0 for PtNi model, which is consistent with the experimental data and given that most Ga dopants are located on the surface of PtNi in reality, only Ga-PtNi models with Ga on the top surface layer were considered. For the oxygen adsorption calculations, we investigated all possible adsorption sites but the most stable adsorption site was reported here for discussion.

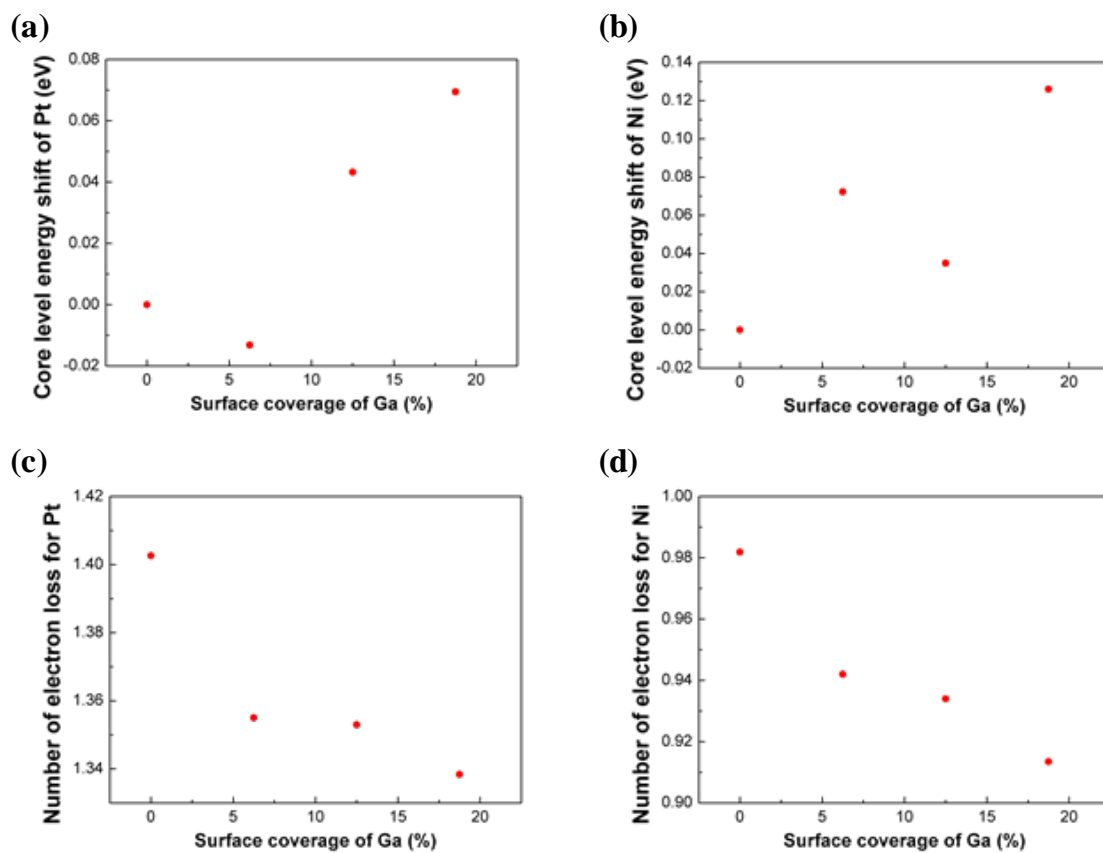


Figure S9. Core-level energy shift of (a) Pt and (b) Ni, and number of electron loss for (c) Pt and (d) Ni next to Ga on the surface of Ga-PtNi/C.

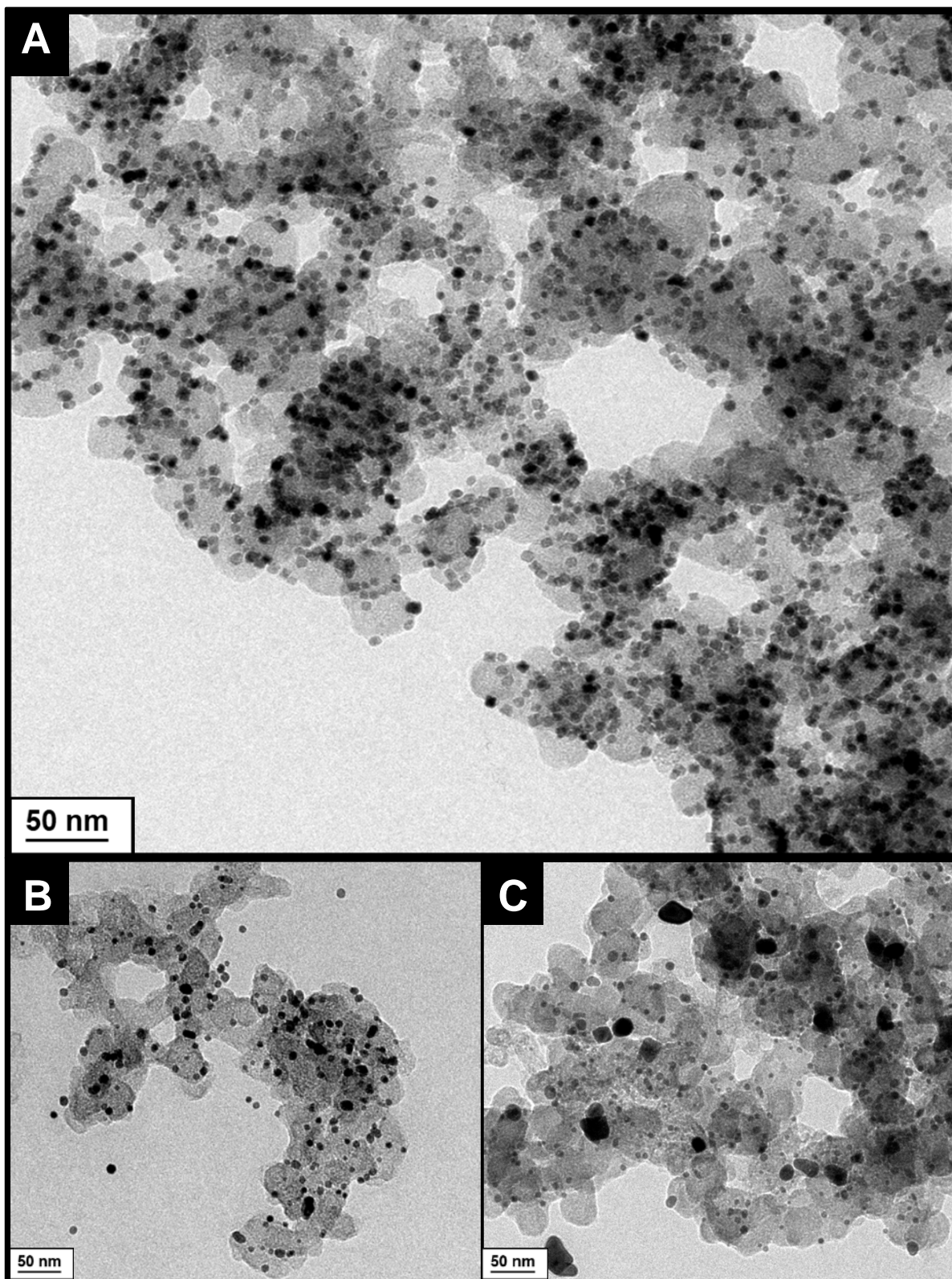


Figure S10. TEM images of (a) Ga-PtNi/C, (b) PtNi/C, and (c) commercial Pt/C from catalyst particles taken from catalyst-coated membranes after 30k durability MEA tests.

References

1. Li, Y.; Quan, F.; Chen, L.; Zhang, W.; Yu, H.; Chen, C. *RSC Advances* **2014**, 4, (4), 1895-1899.
2. Huang, X.; Zhao, Z.; Cao, L.; Chen, Y.; Zhu, E.; Lin, Z.; Li, M.; Yan, A.; Zettl, A.; Wang, Y. M. *Science* **2015**, 348, (6240), 1230-1234.
3. Choi, J.; Lee, Y.; Kim, J.; Lee, H. *Journal of Power Sources* **2016**, 307, 883-890.
4. Gatalo, M.; Jovanović, P.; Polymeros, G.; Grote, J.-P.; Pavlišić, A.; Ruiz-Zepeda, F.; Šelih, V. S.; Šala, M.; Hočvar, S.; Bele, M. *ACS Catalysis* **2016**, 6, (3), 1630-1634.
5. Beermann, V.; Gocyla, M.; Willinger, E.; Rudi, S.; Heggen, M.; Dunin-Borkowski, R. E.; Willinger, M.-G.; Strasser, P. *Nano letters* **2016**, 16, (3), 1719-1725.
6. Blöchl, P. E. *Physical review B* **1994**, 50, (24), 17953.
7. Kresse, G.; Furthmüller, J. *Physical review B* **1996**, 54, (16), 11169.
8. Hammer, B.; Hansen, L. B.; Nørskov, J. K. *Physical Review B* **1999**, 59, (11), 7413.
9. Fishman, M.; Zhuang, H. L.; Mathew, K.; Dirschka, W.; Hennig, R. G. *Physical Review B* **2013**, 87, (24), 245402.